Experimental determination of the ^{41}Ca(n,α)^{38}Ar reaction cross section up to 80 keV, and calculation of the Maxwellian averaged cross section at stellar temperatures

S. Vermote, C. Wagemans, and L. De Smet[*]

Department of Physics and Astronomy, University of Gent, Proeftuinstraat 86, B-9000 Gent, Belgium

C. Lampoudis and J. Van Gils

EC-JRC-IRMM, Neutron Physics Unit, Retieseweg 111, B-2440 Geel, Belgium

The ^{41}Ca(n,α)^{38}Ar reaction cross section was studied at the linear accelerator GELINA of the Institute for Reference Materials and Measurements in Geel (Belgium) and was determined up to a neutron energy of about 80 keV using the time-of-flight technique. In this energy region, 15 resonances were observed, whereas none were identified before. For some of them, resonance parameters such as resonance energy, total width, area, and spin could be determined. From the obtained cross-section data, Maxwellian averaged cross sections have been calculated at various stellar temperatures for further use in stellar models.

PACS number(s): 25.40.Fq, 27.40.+z, 97.10.Cv

I. INTRODUCTION

^{41}Ca is a long-lived nucleus (half-life about 0.1 Myr) produced via neutron capture on ^{40}Ca in AGB stars. The neutrons originate from the ^{22}Ne(α,n)^{25}Mg reaction, which activates at about 300 MK [1]. The predominant destruction process is the ^{41}Ca(n,α)^{38}Ar reaction, thus a good knowledge of its Maxwellian averaged cross section (MACS) at about 300 MK (25 keV) is essential for the calculation of the ^{41}Ca production balance.

The ^{41}Ca(n,α) reaction is also important to answer the question about the origin of ^{36}S, an isotope believed to be synthesized during the s process and in particular during the weak s process. Calculations by Beer and Penzhorn [2] adopted a phenomenological approach in the so-called classical model. More recently, Schatz *et al.* [3] and Reifarth *et al.* [4] performed network calculations on the basis of increasingly realistic stellar models of massive stars for describing the weak s process. Here the s process occurs in two steps: core He burning at kT = 25 keV and shell C burning at kT = 90 keV. Both references [3,4] include a sensitivity analysis of the most relevant cross sections in the network, demonstrating the importance of the ^{41}Ca(n,α)^{38}Ar reaction. This is also illustrated in Fig. 1, which shows the s process nucleosynthesis network in the mass region between $28 \leqslant A \leqslant 42$. It can be seen that the reaction ^{41}Ca(n,α)^{38}Ar reaction recycles to ^{36}S via the reaction chain ^{41}Ca(n,α)^{38}Ar(n,γ)^{39}Ar(n,α)^{36}S.

The ^{39}Ar(n,α)^{36}S channel is included in the stellar models and the ^{41}Ca(n,α)^{38}Ar reaction is considered as the most important neutron-induced reaction on ^{41}Ca in the temperature range of the weak s process. Already in 1978 Woosley *et al.* [5] predicted that the ^{41}Ca(n,α) reaction strongly dominates over the ^{41}Ca(n,γ) reaction in the neutron resonance region. As a consequence, the Maxwellian averaged cross section (MACS) at stellar temperatures of importance for s-process nucleosynthesis in stars will be larger for the ^{41}Ca(n,α)

reaction than for ^{41}Ca(n,γ). This will cause a branching in the nucleosynthesis path. To verify theoretical MACS values (e.g., calculated by Goriely *et al.* [6] and Rauscher *et al.* [7]), a dedicated measurement of the ^{41}Ca(n,α)^{38}Ar reaction cross section as a function of the neutron energy was performed from a few eV up to about 80 keV. Partial results have already been reported in [8–10].

## II. EXPERIMENTAL SETUP AND DATA REDUCTION

A. Experimental setup

The ^{41}Ca(n,α)^{38}Ar reaction was studied at the GELINA neutron time-of-flight facility of the Institute for Reference Materials and Measurements (IRMM) in Geel (Belgium). The linear accelerator produces a pulsed electron beam. The high-energy electrons hit a cooled and rotating uranium target, in which they are slowed down and generate Bremsstrahlung γ rays. The neutrons are then produced via (γ,n) and (γ,f) reactions. To increase the number of slow neutrons, two water-filled beryllium moderators are placed above and below the uranium target. The resulting neutron energy distribution can be characterized by a Maxwellian distribution at thermal energy and a high energy tail with approximately a 1/E shape. The neutron energy spectrum ranges from a few meV up to a few MeV. The time-of-flight method (TOF) is applied to determine the energy of the interacting neutrons. More detailed information about the GELINA facility can be found in Refs. [11,12].

Two different measurement campaigns were performed to define the reaction cross section. One at a 8.5-m-long flight path and a second one at a 30-m-long flight path to improve the energy resolution and to extend the energy range.

The accelerator was operated at a repetition frequency of 800 Hz, and the electron bursts had a width of 1 ns. To remove neutrons from previous bursts, a cadmium overlap filter at 8.5 m and a boron overlap filter at 30 m were permanently used in the neutron beam. The time-dependent background

*liesbeth.desmet@gmail.com
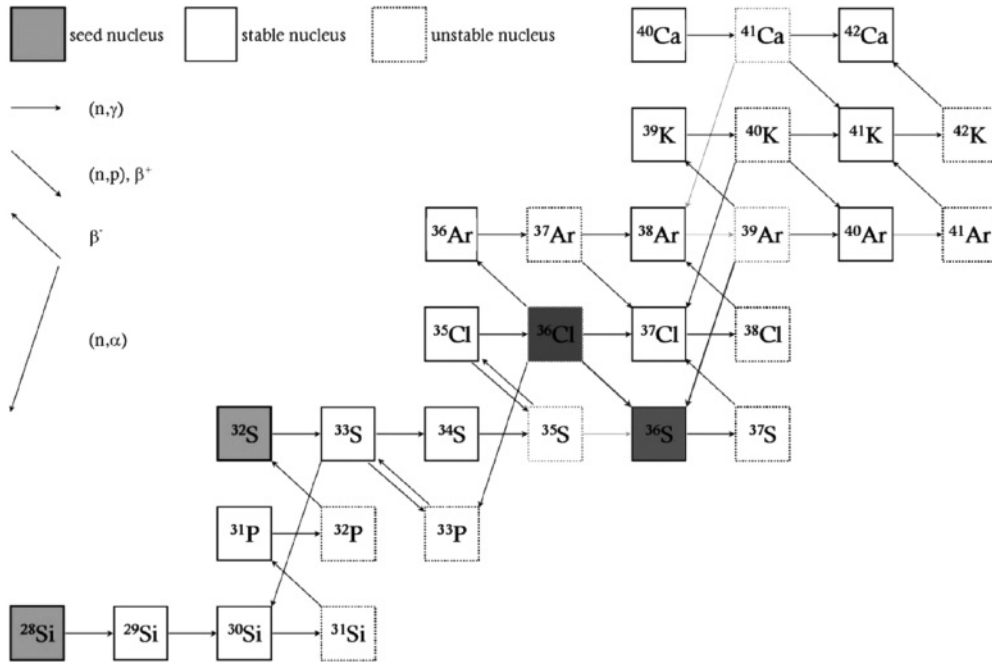
FIG. 1. *s*-process synthesis path in the mass region $28 \leqslant A \leqslant 42$.

was determined in a separate measurement by putting black resonance filters such as Au, Co, Mn, Rh, W, and Al in the neutron beam. The thickness of each filter is chosen in such a way that all neutrons with the energy of (at least one) strong resonance are absorbed, so the measured counting rate at that energy is because of background.

For the detection of the α particles, a Frisch gridded ionization chamber filled with ultrapure methane as detector gas was used, leading to a 2π detection geometry.

For neutron-induced charged particle reactions on ^{41}Ca, both (n,p) and (n,α) reactions are possible, as shown in the level scheme (Fig. 2). The presence of (n,α_0), (n,α_1), $(n,\gamma\alpha)$, and (n,p) transitions was clearly demonstrated with thermal neutrons by Wagemans *et al.* [13]. However, the settings of the ionization chamber were adjusted to detect only the α particles. Figure 3 shows the anode spectrum, measured at the 8.5-m-long flight path, for the four biggest resonances appearing in the TOF spectrum, showing the intervals where the α_0, α_1, and $\gamma\alpha$ particles occur.

The signals from the anode and cathode were amplified and sent to an analog-to-digital converter (ADC). A third signal was sent from the amplifier on the cathode side to a timing single channel analyzer (TSCA). If this signal lies between some predefined levels, a fast logic signal t_n is sent to a time coder (TC) and serves as a stop signal. The start signal t_0 is generated by the linear accelerator and is sent to the time coder just before the electrons impinge on the uranium target. The TC measures the time difference between t_n and t_0 for each event and converts it into a TOF channel number. At this point, both ADC and TOF channel numbers are handled by the LABVIEW-based data acquisition system 2000-DAQ developed at the IRMM [14] and are stored on a PC for off-line analysis.

Two different ^{41}Ca samples were used for the measurements, both prepared at the IRMM by suspension spraying in

methanol on an aluminum foil. Details about the two samples can be found in Table I. The number of ^{41}Ca atoms in the samples was obtained after a careful new measurement of the 3.6-keV KX rays emitted by ^{41}Ca after electron conversion, using a dedicated detector [15]. The uncertainty is mainly because of the uncertainty on the ^{41}Ca half-life, for which a value of $(1.02 \pm 0.07) \times 10^5$ year is adopted [16]. The CaF_2 sample has the higher enrichment in ^{41}Ca; moreover, α particles lose less energy in CaF_2 than in $CaCO_3$, resulting in a better energy resolution. A perfect separation of the α_0 and α_1 particles is only possible with the CaF_2 sample, as shown in Fig. 2. Unfortunately, the CaF_2 sample contains about 10 times less atoms than the $CaCO_3$ sample. Therefore this sample could not be used at the 30-m-long flight path, because there the counting rate is about 10 times lower than at 8.5 m. For the neutron flux determination a ^{10}B layer was used, containing $(8.51 \pm 0.43) \times 10^{19}$ atoms for the measurement at 30 m, and $(7.17 \pm 0.13) \times 10^{19}$ atoms for the 8.5-m measurement.

B. Data reduction

The total observed counting rate $Y_{Ca}(E_n)$ for the ^{41}Ca(n,α) reaction as a function of the neutron energy is

$$Y_{Ca}(E_n) = \varepsilon_{Ca} N_{Ca} \sigma_{Ca}(E_n)\varphi(E_n) + Y_{Ca}^{BG}(E_n),$$

where ε_{Ca} is the detector efficiency and N_{Ca} the number of atoms in the ^{41}Ca sample used. $\sigma_{Ca}(E_n)$ is the differential neutron-induced cross section to be determined and $\varphi(E_n)$ represents the neutron flux. The time-dependent background Y_{Ca}^{BG} was determined as a function of the time-of-flight t by fitting a function,

$$Y_{Ca}^{BG}(t) = at^b + c,$$
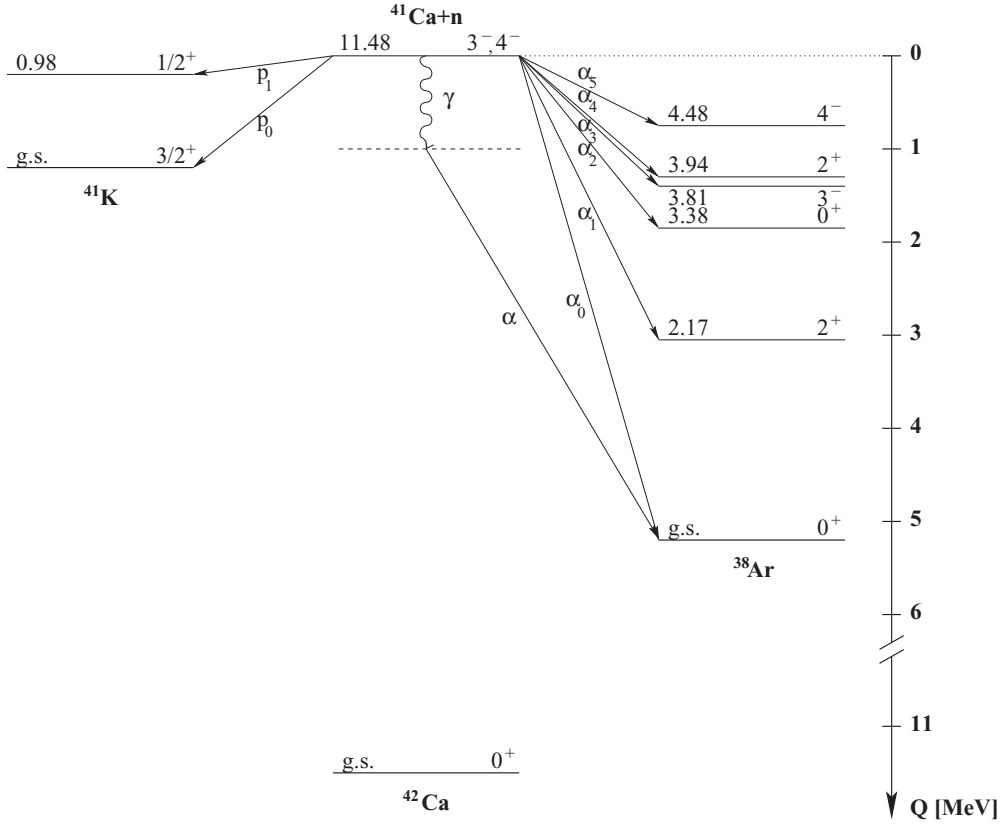
FIG. 2. Level scheme for the ^{41}Ca$(n,p_i)^{41}$K and ^{41}Ca$(n,\alpha_i)^{38}$Ar reactions. The energies are in MeV.

through the counting rates in the black resonance regions. Then, the background was subtracted from the counting rate $Y_{Ca}(t)$ after normalization to the same integrated neutron flux. An identical relation for the flux counting rate, in our case the ^{10}B(n,α) counting rate, is adopted and dividing them

gives

$$\sigma_{Ca}(E_n) = \frac{\varepsilon_B}{\varepsilon_{Ca}} \frac{Y_{Ca}(E_n) - Y_{Ca}^{BG}(E_n)N_B}{Y_B(E_n) - Y_B^{BG}(E_n)N_{Ca}} \sigma_B(E_n).$$

Because the ^{41}Ca(n,α) reaction and the ^{10}B(n,α) reaction have been measured in the same experimental conditions, $\varepsilon_B/\varepsilon_{Ca} = 1$ (detection geometry equals 2π). The known ^{10}B(n,α) reference cross section $\sigma_B(E_n)$ is taken from the ENDF/B-VII database [17].

III. RESULTS

A. Cross section

The data have been analyzed using AGS, a computer code for data analysis and uncertainty propagation in time-of-flight cross-section data, which was developed at IRMM [18,19]. It takes into account the different sources of uncertainty and takes care of the uncertainty propagation during the
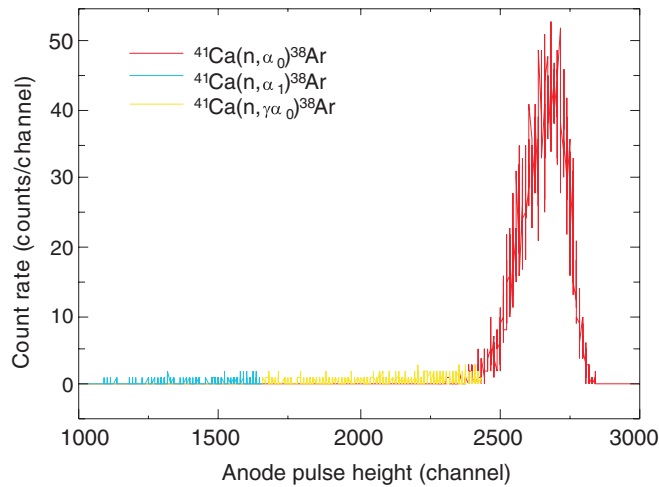

FIG. 3. (Color online) Anode spectrum, measured at the 8.5-m-long flight path, for the four biggest resonances appearing in the TOF spectrum. The intervals where the different α particles occur are represented with a different color.

TABLE I. Characteristics of the ^{41}Ca samples used.

Flight path	Material	Enrichment (%)	Effective area (cm^2)	Number of atoms
8.5 m	CaF$_2$	81.69	6 × 5	$(3.23 \pm 0.32) \times 10^{17}$
30 m	CaCo$_3$	63.38	6 × 5	$(4.08 \pm 0.40) \times 10^{18}$

data reduction steps, producing an experimental covariance matrix. The sources of uncertainties that influence the accuracy of the data can be divided in three categories: statistical uncertainties, overall normalization uncertainties, and neutron energy-dependent systematic uncertainties. Statistical uncertainties are depending on the cross sections of the measured reactions, and, as a consequence, strongly vary with neutron energy. In the analysis, the statistical uncertainties for the ^{41}Ca and ^{10}B measurements have been taken into account. The overall normalization uncertainty of the data is determined
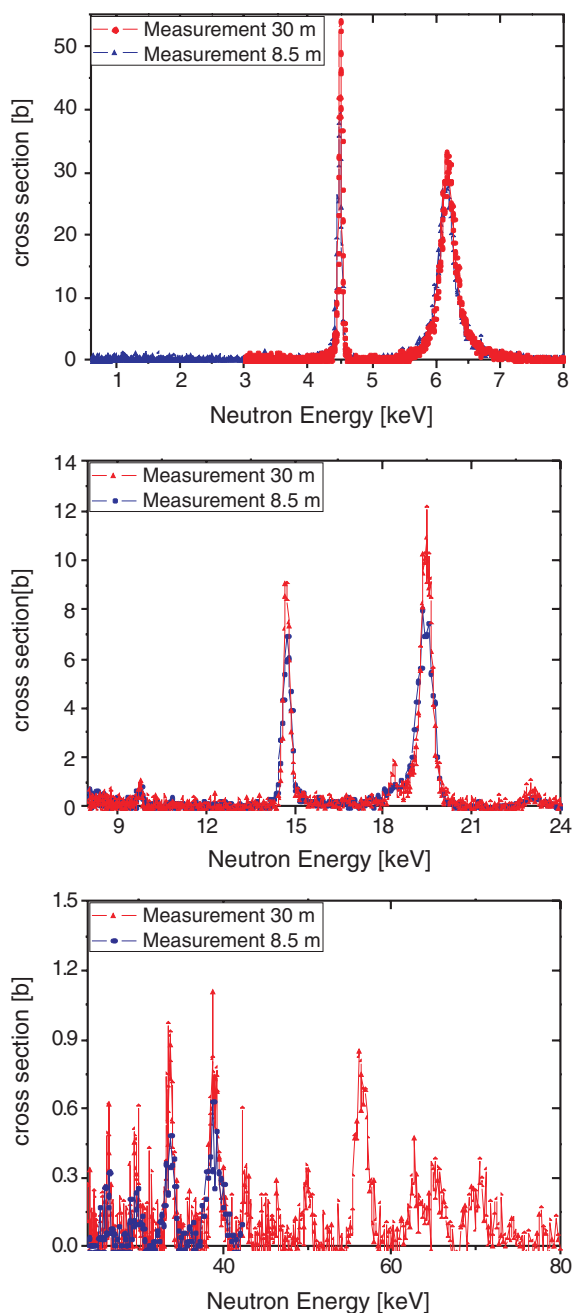
by the uncertainties on the number of atoms in the ^{41}Ca and ^{10}B samples used. Apart from the uncertainty on the overall normalization of the data, there is the uncertainty on the correction for the time-dependent background which consequently depends on the neutron energy.

Figure 4 shows the ^{41}Ca$(n,\alpha)^{38}$Ar cross section for both measurements. From the measurement at 30 m, results are obtained from 3 to 80 keV, while the 8.5-m measurement gives results from 600 to 40 keV. This figure clearly demonstrates that the energy resolution of the measurement at a 30-m-long flight path is better than for the results obtained at 8.5 m. The double resonance around 19 keV shows now two well-separated resonances, which can be fitted separately.

The ^{41}Ca$(n,\alpha)^{38}$Ar cross-section data obtained in this work are available in the Experimental Nuclear Reaction Data (EXFOR) data base of the Nuclear Energy Agency in Paris.

B. Resonance analysis

1. Fitting procedure

The broadening of resonances from the experimental resolution has a strong influence on the accuracy of the fitted resonances. Contributions to the experimental resolution are for example, the Doppler broadening, time resolution of the detector, and the time distribution of the neutron source. In first approximation this resolution can be expressed as a Gaussian function.

For the first measurement at a 8.5-m-long flight path, this was done by using the Voigt expression. A Voigt shape is a convolution of a Gauss and a Breit-Wigner function, where the Gaussian contribution represents the experimental broadening, and the Breit-Wigner part represents the natural line width.

The parameters that could be obtained from the Voigt fits are the resonance energy E_{res} and the area of the resonance A_{res}. Furthermore, values for the total width Γ are obtained, however, with large uncertainties. For each resonance, all these

FIG. 4. (Color online) ^{41}Ca(n,α) cross section between 3- and 80-keV neutron energy. The red line shows the results of the measurement at a 30-m-long flight path; the blue curves are the data measured at a 8.5-m-long flight path.

TABLE II. Resonance parameters obtained from the Voigt fits for the measurement at the 8.5-m-long flight path.

Energy (eV)	Area (b.eV)	Γ (eV)
1090 ± 70	30 ± 15	
4490 ± 10	3400 ± 300	40 ± 20
6170 ± 60	11350 ± 950	260 ± 26
9725 ± 75	170 ± 60	125 ± 100
14725 ± 75	2500 ± 300	175 ± 140
18450 ± 300[a]	–	–
19430 ± 150	5800 ± 600	420 ± 100
23080 ± 200	400 ± 150	600 ± 200
26100 ± 800[b]		
29700 ± 700	250 ± 100	1250 ± 1000
33700 ± 700	550 ± 220	1000 ± 600
38850 ± 1200	900 ± 300	2000 ± 1200

[a]The resonance at 19.43 keV is a double resonance with a first level at 18.45 keV.

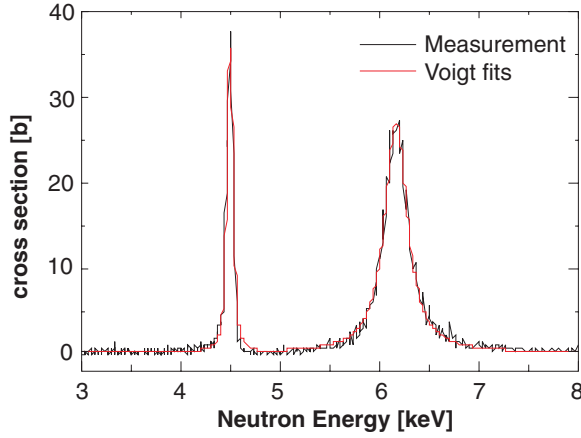[b]Too low counting statistics, so the area has not been fitted.

FIG. 5. (Color online) Voigt fits to the ^{41}Ca(n,α) cross-section data for some resonances, measured at the 8.5-m-long flight path.
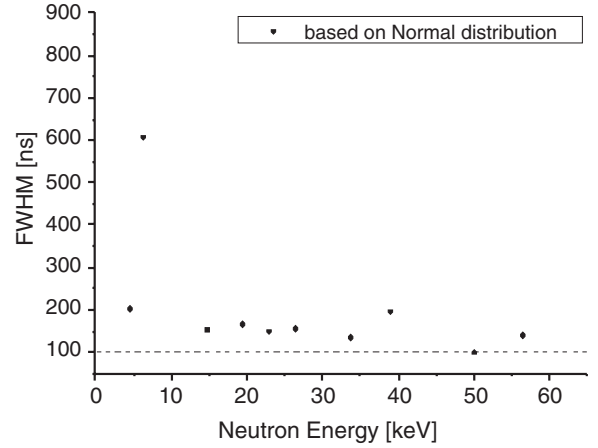

FIG. 6. The total broadened width for the most prominent resonances. The dashed line represents the experimental broadening.

values are listed in Table II. The resulting Voigt fits are shown in Fig. 5 for the resonances at 4.49 and 6.17 keV.

For the 30-m data, a different analysis method was chosen. In this case the resonance shape analysis code SAMMY [20], which is based on the Reich-Moore approximation of the *R*- matrix theory, was employed. SAMMY code can account accurately for the various components of the experimental resolution. The total width Γ, can be reliably determined from the experimental data, if the natural line width is of similar magnitude as the experimental broadening. Figure 6 shows the extracted total width (natural plus experimental) of the resonances, in comparison to the experimental resolution level (dashed line). Therefore it can be concluded that a resonance shape analysis is only feasible for the case of the first two resonances (the resonance at about 40 keV has too low statistics). For all other resonances only the area can be deduced.

Furthermore the resonance strength ω_α can be calculated from the resonance area using the formula,

$$\omega_\alpha = \frac{k_{\text{res}}^2}{2\pi^2} A_{\text{res}},$$

with

$$k_{\text{res}}^2 \left[\frac{1}{b}\right] = 4.826 \times 10^{-6} E_{\text{res}}(\text{eV})$$

Ref. [21]. All these results are listed in the left part of Table III. Figure 7 shows the fits performed with SAMMY for the first two resonances at 4.5 and 6.2 keV, for which also Γ could be determined, as well as the fits for two resonances at higher energies, namely 19.5 and 56.5 keV.

2. Spin assignment

The spin assignments mentioned here are done based on the measurement at the 8.5-m-long flight path, where the thin ^{41}Ca sample could be used. *s*-wave (l = 0) neutrons impinging on ^{41}Ca, ground state $I^\pi = 7/2^-$, will populate the $J^\pi = 3^-$ and $J^\pi = 4^-$ states of the compound nucleus ^{42}Ca, whereas *p*-wave (l = 1) neutrons can populate states from $J^\pi = 2^+$ through $J^\pi = 5^+$. The formed states decay to the ground

TABLE III. (Left part) Resonance parameters obtained with SAMMY for the measurement at the 30-m-long flight path. (Right part) $\Gamma_{\text{n}}/\Gamma_{\text{p}}$ values for the resonances observed in this work which correspond to resonances observed by Meijer and Van Gasteren [22].

Energy (eV)	Γ (eV)	Area (b.eV)	ω_α (eV)	ω_{p} (eV) [20]	$\frac{\Gamma_n}{\Gamma_p}$
4500 ± 2	36 ± 4	3573 ± 165	3.93 ± 0.18	7.4	8.50 ± 0.39
6183 ± 5	245 ± 13	11709 ± 367	17.70 ± 0.56	–	–
9753 ± 65	–	170 ± 125	0.41 ± 0.30	9.2	0.71 ± 0.52
14730 ± 14	–	2898 ± 328	10.44 ± 1.18	–	–
18363 ± 74	–	523 ± 235	2.35 ± 1.06	–	–
19467 ± 15	–	5906 ± 389	28.11 ± 1.85	1.6	281.1 ± 18.49
23011 ± 92	–	224 ± 129	1.26 ± 0.73	2.8	7.2 ± 4.14
26408 ± 119	–	184 ± 113	1.19 ± 0.73	–	–
29659 ± 144	–	185 ± 98	1.34 ± 0.71	7.1	3.02 ± 1.60
33676 ± 135	–	664 ± 263	5.47 ± 2.17	5.7	15.35 ± 6.08
38941 ± 301	–	1211 ± 497	11.53 ± 4.73	2.9	63.61 ± 26.09
42598 ± 237	–	264 ± 154	2.74 ± 1.60	1.1	39.85 ± 23.30
50028 ± 297	–	299 ± 156	3.66 ± 1.91	6.9	8.49 ± 4.42
56444 ± 241	–	1177 ± 366	16.24 ± 5.05	–	–

($J^\pi = 0^+$) or first excited state ($J^\pi = 2^+$) of ^{38}Ar by emitting α_0 or α_1 particles, respectively. The smallest allowed angular momenta of the emitted α particles are tabulated in Table IV.

Wagemans *et al.* [13] measured the ^{41}Ca(n_{th},α_i) reaction cross section with thermal neutrons at the ILL in Grenoble. This thermal cross section is the sum of the tails of all *s*-wave resonances. From the fitted total natural line width and from the fitted area, the contribution from each resonance to the thermal cross section can be calculated with the formula:

$$\sigma(E_{th}) = \frac{1}{2\pi \sqrt{E_{th}}} \frac{\Gamma_{res} A_{res}}{E_{res}^{2/2}}.$$

If this calculated value is higher than the measured thermal cross section, the resonance is taken as a *p* wave. On the basis of this calculation it is concluded that only the resonances around 1.1 and 10 keV may be *s* wave. Although the natural line width could not be determined for the resonance at 1.1 keV, it can be deduced from the resonance area that its thermal contribution in case of an *s* wave will not exceed the measured thermal cross section. The pulse height spectra (anode and cathode) for the resonance at 1.1 keV reveal that only α_1 particles are observed, so this is a transition only to the first

excited state of ^{38}Ar. Taking into account the spin assignments for *s*-wave neutrons, the only possibility is that this resonance corresponds to a 4^- state of ^{42}Ca. On the contrary, the 10-keV resonance consists of (n,α_0) as well as (n,α_1) transitions. With the help of Table IV, it is concluded that the 10-keV resonance is a 3^- state in ^{42}Ca. All the other resonances are considered to be *p* wave. Because (n,α_0) and (n,α_1) transitions are observed in all of them, these resonances are most probable 2^+ states as 3^+ and 5^+ states are ruled out by parity constraints and the 4^+ state is less probable because the higher orbital momentum of the α particle reduces the penetrability through the centrifugal barrier.

3. Determination of the partial level widths

The only additional information on ^{42}Ca compound levels in the covered energy range was obtained in a proton-induced reaction on ^{41}K by Meijer and Van Gasteren [22]. They reported a list of $\omega_p = (2J+1)\Gamma_p\Gamma_{\alpha0}/\Gamma$ values for the measured ^{41}K$(p,\alpha_0)^{38}$Ar reaction. The Γ_P value from their work corresponds with p_0 decay in the case of neutron-induced reactions on ^{41}Ca. In the case of a neutron-induced reaction on
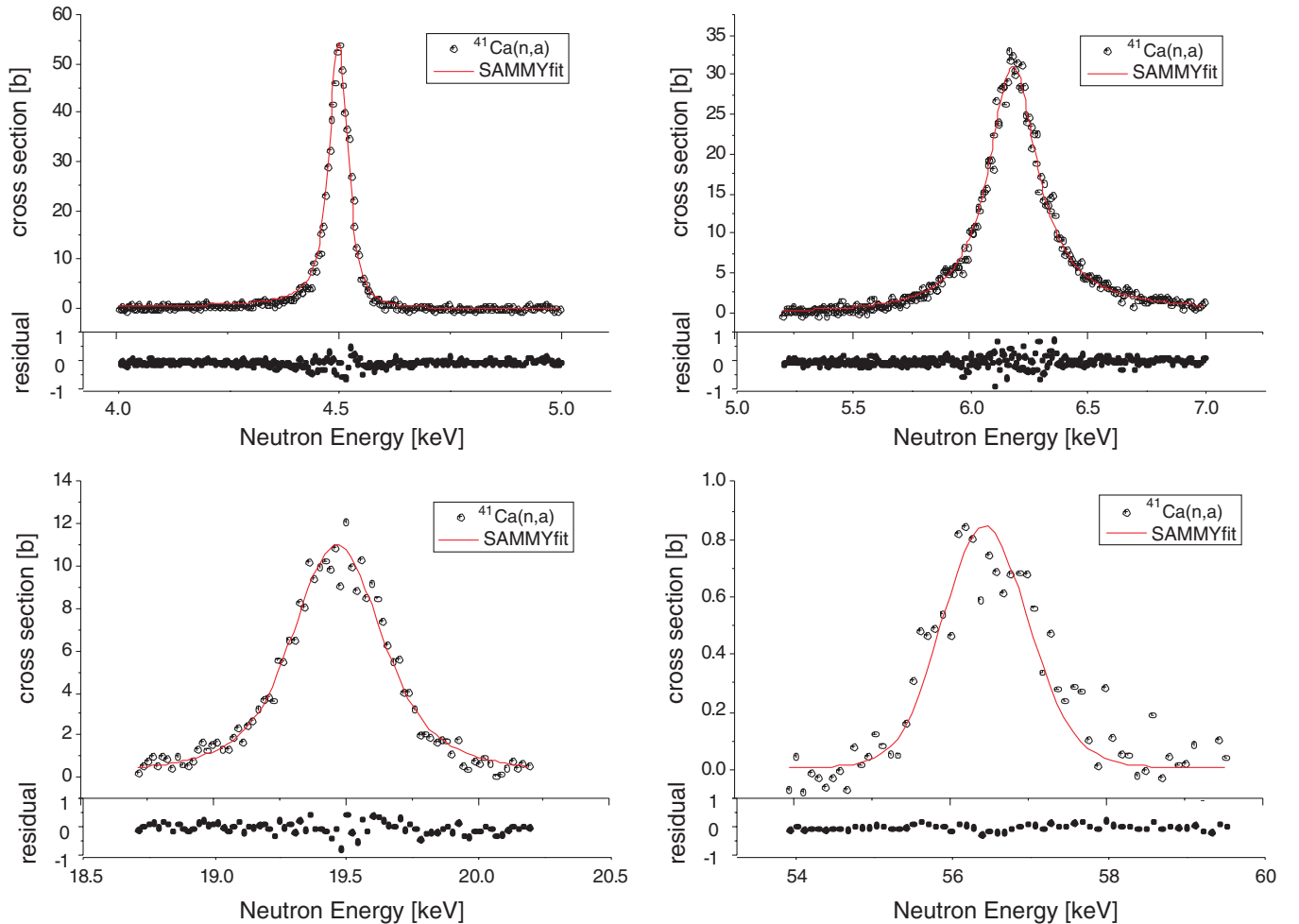

FIG. 7. (Color online) SAMMY fits to the ^{41}Ca(n,α) cross-section data for the first two resonances (upper part) and for the resonances at 19.5 and 56.5 keV (lower part), measured at the 30-m-long flight path. The residuals are shown as well.

TABLE IV. Smallest allowed angular momenta of the emitted α particles from the formed compound nucleus ^{42}Ca in the case of impinging s- or p-wave neutrons.

$J^{\pi\,38}$Ar	$J^{\pi\,42}$Ca compound nucleus					
	s wave		p wave			
	3^-	4^-	2^+	3^+	4^+	5^+
0^+ (α_0)	3	p.f.	2	p.f.	4	p.f.
2^+ (α_1)	1	3	0	2	2	4

^{41}Ca only p_0 and p_1 decay to ^{41}K is possible (see Fig. 2), so $\Gamma_p = \Gamma_{po} + \Gamma_{p1}$. However, the probability that the p_1 particles penetrate the Coulomb barrier is very low because their energy is only 0.21 MeV. Therefore, it can be assumed that $\Gamma_p = \Gamma_{p0}$ in a neutron-induced measurement. Consequently, the Γ_p from the measurement of Meijer and Van Gasteren [22] is equal to the Γ_p from this work. By dividing the fitted resonance strength ω_α obtained in this work ($\omega_\alpha = g\Gamma_n\Gamma_\alpha/\Gamma$ with $g = (2J + 1)/16$), by the reported ω_p value of Meijer and Van Gasteren, a value for Γ_n/Γ_p is obtained. The values for Γ_n/Γ_p for the resonances obtained in this work which correspond to resonances observed by Meijer and Van Gasteren [22] are listed in Table III.

The partial widths may be calculated through combining the expressions for ω_p and ω_α mentioned above, and the expression for the total width $\Gamma = \Gamma_n + \Gamma_\gamma + \Gamma_p + \Gamma_\alpha$. Five parameters ($J$, Γ_n, Γ_γ, Γ_p, and Γ_α) have to be fixed with only three equations at our disposal. This means that it is not possible to solve this system of equations unambiguously. For this reason no partial level widths could be determined. Additional measurements leading to the same compound nucleus ^{42}Ca are necessary to determine the partial widths.

IV. ASTROPHYSICAL IMPLICATIONS

A. Determination of the MACS

Numerical integration of the obtained (n,α) cross-section data of the two measurements using

$$\langle\sigma\rangle = \frac{2}{\sqrt{\pi}}\frac{1}{(kT)^2}\int_0^{+\infty}\sigma(E_\mu)E_\mu e^{-\frac{E_\mu}{kT}}\,dE_\mu,$$

with E_μ the center-of-mass neutron energy, leads to the ^{41}Ca(n,α) MACS values.

In this work, the (n,α) cross section determination reached an energy $E_f \approx 45$ keV for the measurement at 8.5 m and 80 keV for the measurement at 30 m, which means that the integration upper limit of $+\infty$ in the previous formula is replaced by 45 and 80 keV, respectively.

Figure 8 shows the MACS values calculated this way, with the data obtained from the measurement at 8.5 m in blue and the 30-m data in red. Both results are in perfect agreement up to about 20 keV; above this value, the 30-m results are somewhat higher. This is in accordance with expectations, because a resonance at an energy E_{res} has its maximum contribution to the MACS at $kT = E_{res}/2$. This means that, if the cross section is known up to an energy E_f, MACS values above $E_f/2$ are
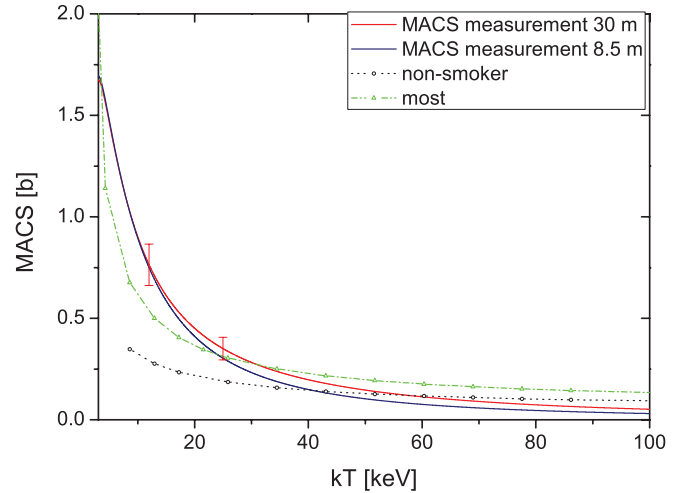

FIG. 8. (Color online) The ^{41}Ca(n,α)^{38}Ar MACS values obtained by numerical integration of the obtained cross-section data. A comparison is made with theoretical values.

mainly originating from resonances at energies higher than E_f. Therefore, the calculated MACS values should be regarded as lower limits above $E_f/2$, that is, above 22 keV for the measurement at 8.5 m and above 40 keV for the measurement at 30 m.

In Fig. 8 a comparison is also made between the experimental values obtained in our two measurements and the theoretical values from the MOST [6] and NON-SMOKER [7] codes. Furthermore, in Table V numerical MACS values are given for a series of relevant thermal energies. From these data it is clear that the MACS values at lower energies obtained in this work are larger than both theoretical values. At 25 and 30 keV, however, the MOST values perfectly agree with our experimental result obtained at 30 m.

The MACS values up to 30 keV calculated from our experimental data can be used in stellar model calculations to calculate the ^{41}Ca production balance and to trace the origin of ^{36}S. In the latter case, for s-process calculations in massive stars, we only obtained a lower limit for the MACS at $kT = 90$ keV.

TABLE V. Numerical MACS values for a series of relevant thermal energies.

kT (keV)	This work (b)	MOST (b)	NON-SMOKER (b)
5	1.46	1.06	–
8	1.08	0.74	–
10	0.90	0.62	0.32
15	0.61	0.45	0.26
20	0.45	0.36	0.22
23	0.39	0.33	0.20
25	0.35	0.31	0.19
30	0.28	0.28	0.17

V. CONCLUSION

In the present work the ^{41}Ca$(n,\alpha)^{38}$Ar reaction cross section was determined from a few eV up to approximately 80 keV. Fifteen resonances were identified. For each of them the resonance position and the area have been determined. For two of them the total level width could be obtained. Additionally, for some resonances the spin could be determined. The calculated MACS values can be used in stellar model calculations to trace the origin of ^{36}S and to calculate the ^{41}Ca production balance.

[1] M. Lugaro and A. Chieffi, in *Lecture Notes in Physics 812* (Springer, New York, 2011), p. 83.

[2] H. Beer and R.-D. Penzhorn, Astron. Astrophys. **174**, 323 (1987).

[3] H. Schatz *et al.*, Phys. Rev. C **51**, 379 (1995).

[4] R. Reifarth *et al.*, Ap. J. **528**, 573 (2005).

[5] S. Woosley *et al.*, At. Data Nucl. Data Tables **22**, 371 (1978).

[6] S. Goriely, http://www-astro.ulb.ac.be/Html/ncap.html.

[7] T. Rauscher, http://nucastro.org/nonsmoker.html.

[8] L. De Smet, Ph.D. thesis, University of Gent (Belgium), 2006.

[9] L. De Smet *et al.*, in *Proceedings Nuclei in the Cosmos IX* (PoS, International School for Advanced Studies, Trieste, 2006), p. 561.

[10] C. Wagemans, S. Vermote, and J. Van Gils, in *Proceedings Nuclei in the Cosmos XI* (PoS, International School for Advanced Studies, Trieste, 2010), p. 199.

[11] A. Bensussan and J. M. Salome, Nucl. Instr. Methods **155**, 11 (1978).

[12] W. Mondelaers and P. Schillebeeckx, Notiziario neutroni e luce di sincrotrone 11.2, 19 (2006).

[13] C. Wagemans, R. Bieber, H. Weigmann, and P. Geltenbort, Phys. Rev. C **57**, 1766 (1998).

[14] J. Gonzalez, C. Bastian, S. De Jonge, and K. Hofmans, *Modular MultiParameter Multiplexer MMPM. Hardware Description and User Guide*, 1997 IRMM Internal Report GE/R/INF/06/97 (IRMM, Geel, 1997)

[15] D. Reher (private communication).

[16] J. Cameron and B. Singh, Nucl. Data Sheets **94**, 429 (2001).

[17] http://www-nds.iaea.org/endf.

[18] C. Bastian, in *Proceedings of the International Conference on Neutrons in Research and Industry*, Vol. 2867 (The International Society for Optics and Photonics, Bellingham, 1997), p. 611.

[19] C. Bastian, A. Borella, F. Gunsing, J. Heyse, S. Kopecky, G. Noguere, P. Siegler, and P. Schillebeeckx, *PHYSOR-2006* (American Nuclear Society, LaGrange Park, IL, 2006).

[20] N. M. Larson, Oak Ridge National Laboratory Technical Report No. ORNL/TM-9179/R8, 2008 (unpublished).

[21] R. L. Macklin and J. H. Gibbons, Rev. Mod. Phys. **37**, 166 (1965).

[22] R. J. Meijer and J. J. M. Van Gasteren, Nucl. Phys. A **148**, 62 (1970).